case reports

Tumor-Infiltrating Leukocyte Phenotypes Distinguish Outcomes in Related Patients With Pancreatic Adenocarcinoma

Jason M. Link, PhD[1,2]; Shannon M. Liudahl, PhD[3]; Courtney B. Betts, PhD[3]; Shamilene Sivagnanam, MS[4]; Kenna R. Leis, BS[4]; Mary McDonnell, MS[2,5]; Carl R. Pelz, BA[2,4]; Brett Johnson, PhD[5]; Kelly J. Hamman, MS, CGC[1]; Dove Keith, PhD[2]; Jone E. Sampson, MD[1]; Terry K. Morgan, MD, PhD[3,6,8]; Charles D. Lopez, MD, PhD[2,7,8]; Lisa M. Coussens, PhD[2,3,8]; and Rosalie C. Sears, PhD[1,2,8]

INTRODUCTION

Pancreatic ductal adenocarcinoma (PDAC) carries one of the highest mortality risks of all cancers. Most patients present with either metastatic PDAC (50%-60%) or locally advanced tumors (30%-40%), for which the median survival is 5-9 months after diagnosis.[1,2] Outcomes are still suboptimal for the small subset (10%-20%) of patients who present with resectable tumors confined to the pancreas; < 50% of these patients survive 5 years after surgery despite modern adjuvant chemotherapy.[3] Moreover, at autopsy, the disease is metastatic for 88% of recurrences, and > 80% have more than 10 distinct metastatic lesions[4] that are genetically related to the primary tumor[5] and other metastases.[6] These observations indicate that the majority of patients with PDAC harbor nonradiographically evident, micrometastatic disease after resection and that remnant tumor cells evade—or acquire resistance to—adjuvant chemotherapy. Although tropism to specific organs during metastatic spread is still poorly understood, patients with recurrence in the liver or peritoneum[7] survive significantly shorter than patients with recurrent lung metastases.[8-10]

PDAC tumors are commonly classified into two major subtypes: one that shares some features with adenosquamous tumors (squamoid and/or basal) and the other that retains a differentiated, glandular and/or ductal morphology (ductal and/or classical). Squamoid PDAC tumors are more glycolytic,[11,12] more hypoxic,[13] more likely to metastasize,[14,15] recruit inflammatory fibroblasts,[16] and yield a poorer prognosis than ductal tumors.[17-21] Classical subtype tumors are associated with more tumor-infiltrating leukocytes, denser collagen, and better outcomes,[15,22] although significant subtype heterogeneity within tumors[13] complicates the relationship between subtype and outcome.

More cytolytic T cells infiltrate PDAC tumors than most other tumors,[23] but they are ultimately insufficient to control the cancer. Density of tumor-infiltrating T cells is highly variable among PDAC tumors,[24] and abundant $CD8^+$ T cells (along with a high number of neoantigens) can support exceptionally long-term survival.[25] However, T cell–mediated tumor immunity may be restricted by several mechanisms: tumor cell downregulation of HLA, immunosuppressive leukocytes, T cell proximity to tumor cells, and T cell exhaustion.[26-30] Effective T cell–mediated tumor immunity is enhanced by a high diversity of functional T cell clones, tumor-specific recruitment of effector T cells, and abundant neoantigens.[23,25,31] Quantifying the phenotypes, functions, and locations of leukocytes is critical to identify specific tumor immunity required for exceptional positive outcomes.

Rare, exceptional control of PDAC progression may be mediated by equally rare, idiosyncratic patient genetics, tumor-specific somatic alterations and gene expression, and/or stochastically generated tumor immunity. In this report, we present the cases of Pt1, who survived more than 46 months with occult, chemotherapy-resistant metastatic PDAC, and her niece (Pt2) who succumbed to progressing metastatic disease despite aggressive treatment. We compare the clinical outcomes and primary and metastatic tumors from these two patients, identifying major differences in subtype, somatic alterations, and leukocyte lineages that—in some combination or alone—might have led to divergent disease courses.

RESULTS

Disparate Outcomes for Two Related Patients Both Diagnosed With Stage II PDAC

Pt1 is a chronic smoker diagnosed at 64 years of age with stage II PDAC (pT3 N1 M0) and treated 26 days later by surgical resection of a moderately to poorly differentiated, invasive ductal adenocarcinoma, followed by two cycles of gemcitabine and capecitabine. A pulmonary lesion measuring 20 mm × 16 mm was evident by CT scan 27 days prior to resection of the primary tumor, but upon biopsy was negative for malignancy. However, during adjuvant chemotherapy, the lung lesion increased to 23 mm × 18 mm, and a CT and/or PET was suspicious for malignancy with a standardized uptake value (SUV) of 4.5. Based on the imaging, the lung lesion was resected and found to be

ASSOCIATED CONTENT

Appendix

Author affiliations and support information (if applicable) appear at the end of this article.

Accepted on December 1, 2020 and published at ascopubs.org/journal/po on February 5, 2021: DOI https://doi.org/10.1200/PO.20.00287

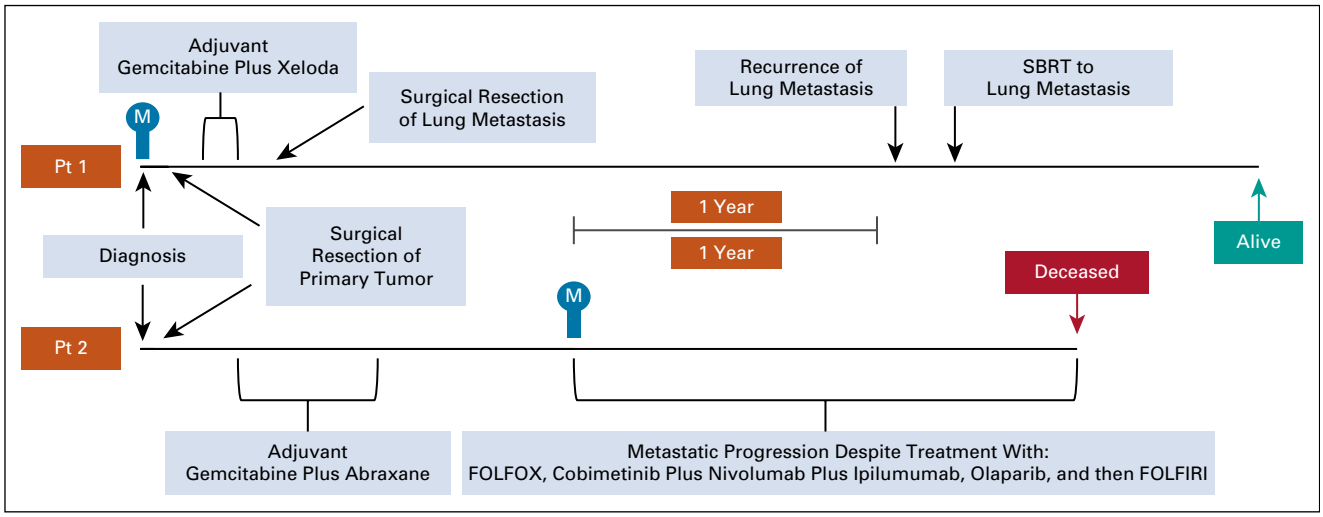

FIG 1. Disease courses for patients 1 (top) and 2 (bottom) aligned by date of diagnosis. The date when metastatic disease was first radiographically evident is indicated with an M in blue. CA19-9 test results are not shown because—for both patients—they were reproducibly approximately 90% lower than the 37 U/mL threshold for normal, even when the primary tumor was present. This result suggests a false negative result because of a Lewis[a-b]- antigen phenotype, as is the case for 5%-10% of Caucasian patients with PDAC.[65]

metastatic PDAC. Pt1 chose to receive no further treatment and was radiographically disease-free for over 2 years (Fig 1) until an isolated, recurrent lung metastasis was identified by CT and FDG-PET (SUV of 9) and then treated by 50 Gy in five fractions using Stereotactic Body Radiotherapy. Four months later, restaging CT revealed that the size of the previously visualized left lower lobe nodule had decreased; there were no additional suspicious lesions, and the patient is asymptomatic 46 months after diagnosis.

Pt2—a nonsmoker—was diagnosed at 44 years of age with stage II PDAC (pT3 N1 M0) and treated by surgical resection of a moderately differentiated adenocarcinoma with squamoid features as described by Hayashi et al[32]—this tumor was not qualified as an adenosquamous subtype of ductal adenocarcinoma. Pt2 was treated with six cycles of gemcitabine and nab-paclitaxel (on a clinical trial). A biopsy-proven, right ureter metastasis in the context of widespread peritoneal metastases was identified 1 year after the last dose of adjuvant chemotherapy, and Pt2 was treated with four cycles of fluorouracil and oxaliplatin. Subsequently, a right retroperitoneal metastasis and multiple liver metastases were identified and continued to progress despite further treatment (Fig 1). Pt2 died 19 months after metastatic disease recurrence.

TABLE 1. Known PDAC Driver Genes Altered in the Primary and Metastatic Tumors From Pt1 and Pt2

	Patient 1		Patient 2	
Gene Altered	**Primary**	**Metastasis**	**Primary**	**Metastasis**
KRAS	p.G12D	p.G12D	p.G12D	p.G12D
TP53	p.L130R	p.L130R	p.R273H	p.R273H
CDKN2A	ND	ND	p.R58*	p.R58*
SMAD4	p.L414*	p.L414*	ND	E520*
PTEN	ND	ND	ND	CNL
RBPJL	ND	ND	p.Y479*	p.Y479*
NOTCH2	ND	ND	ND	CNG
FANCA	ND	p.E1240Q	ND	ND

Abbreviations: CNG, copy number gain; CNL, copy number loss; ND, none detected; PDAC, pancreatic ductal adenocarcinoma.

A Shared Germline *PRSS1* Mutation and Somatic Alterations Common to PDAC

We identified germline *PRSS1* p.A16V in both patients and somatic alterations in the two most common PDAC driver genes—*KRAS* and *TP53*—in both tumors from each patient (Table 1). The primary tumor from Pt2 also contained a *CDKN2A* alteration. Metastatic tumors from both patients had all alterations found in their respective primary tumors. Additionally, the Pt1 metastasis contained an *FANCA* mutation, whereas the Pt2 metastasis contained a *PTEN* deletion. *SMAD4* was altered in both the primary and metastatic tumors from Pt1, but only in the metastasis from Pt2.

Evidence of Squamoid Differentiation in Tumors From Patient 2

The histology of Pt1's primary tumor was homogeneously ductal and did not express KRT5, whereas Pt2's primary tumor contained heterogeneous squamoid features and KRT5 expression in approximately 25% of tumor cells (Fig 2A).[32] The lung metastasis from Pt1 was ductal, whereas the ureter metastasis from Pt2 was mostly squamoid (Fig 2B).

To further distinguish ductal PDAC from squamoid PDAC, we classified the subtype (classical or quasimesenchymal/basal of each tumor using RNASeq and a previously published gene panel [PDAssigner[18]]) and the PurIST

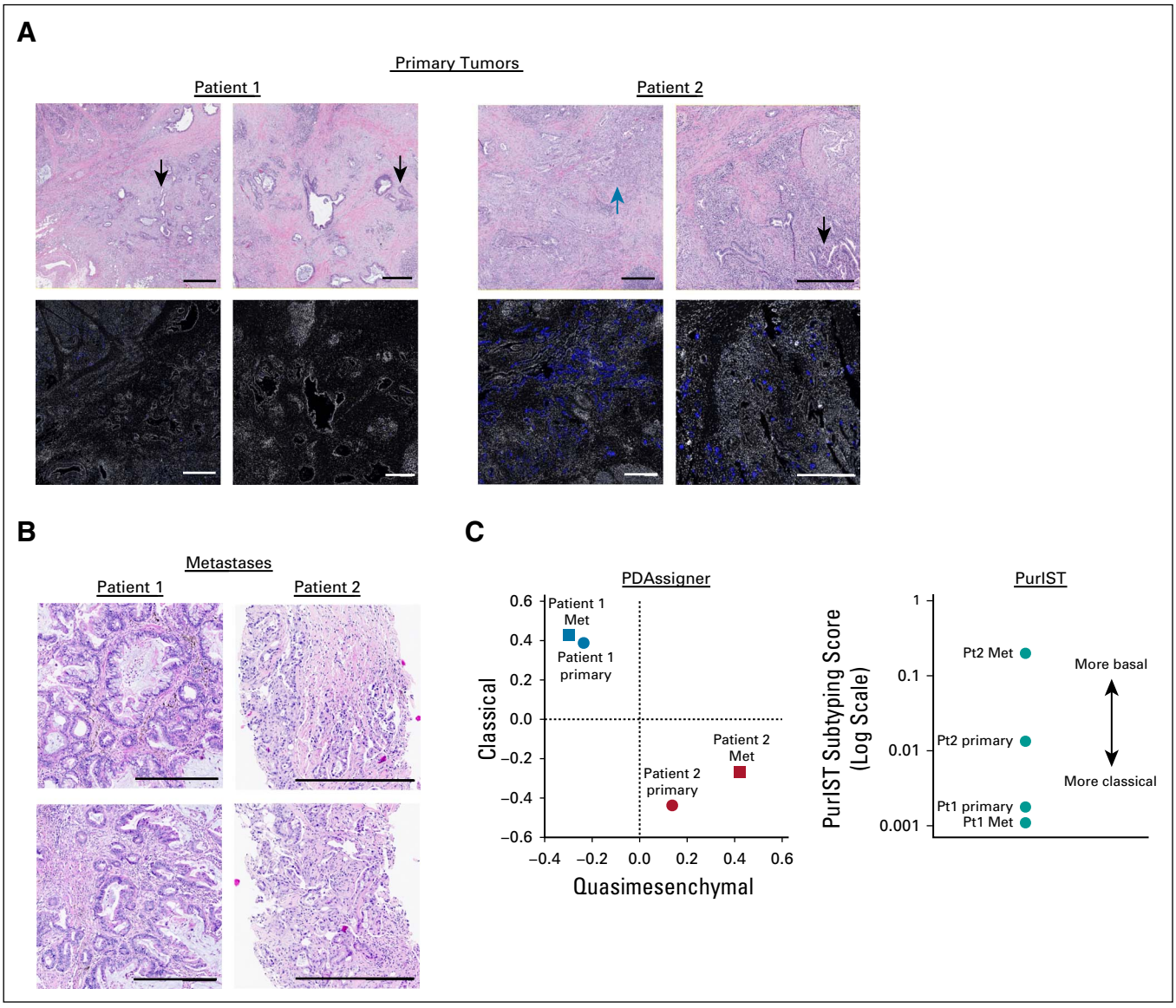

FIG 2. PDAC subtype assignment based on histology and gene expression. (A) H&E stained sections and immunohistofluorescence for KRT5 (blue) and DAPI (white) from primary tumors. Regions of ductal or squamoid histology are indicated by black or blue arrows, respectively. Each scale bar is 0.5 mm. (B) H&E stained sections of metastases from Pt1 (lung) and Pt2 (ureter). Each scale bar is 0.5 mm. (C) PDAC subtyping of each patient's primary and metastatic tumors. Left panel: Spearman correlation coefficients for tumors from Pt1 and Pt2 compared with the published rank order of PDAssigner genes for classical (y-axis) and quasimesenchymal (x-axis) tumors. Right panel: scores from PurIST subtyping for each tumor. PDAC, pancreatic ductal adenocarcinoma.

technique[33] that normalizes differences in tumor cellularity (Fig 2C). Both tumors from Pt1 aligned well with the classical subtype, whereas the tumors from Pt2 were more quasimesenchymal and/or basal with the metastasis scoring more basal than the primary tumor.

Leukocyte Types Associated with Immunity in Tumors From Patient 1

We used a multiplex immunohistochemistry (mIHC) workflow[34] to quantify the densities of tumor cells, fibroblasts, and 10 leukocyte subsets (Appendix Table A1). We compared the primary tumors from both patients with the metastasis from Pt1, but limited material prevented us from analyzing the metastasis from Pt2. We selected regions of interest (ROIs) within each section that contained both KRT$^+$ epithelial or tumor cells and CD45$^+$ immune cells (Appendix Fig A1), followed by quantitative assessment of each ROI. The metastasis from Pt1 had more epithelial or tumor cells than her primary tumor and fewer fibroblasts than the primary tumor from Pt2 (Fig 3A). A detailed analysis of leukocyte subsets revealed that CD8$^+$ T cells and CD4$^+$ T cells were significantly denser in the metastasis from Pt1 compared with the primary tumor from Pt2 (Fig 3B). Additionally, the primary tumor from Pt1 had a lower density of granulocytes and a higher density of Th1-like macrophages compared with the primary tumor from Pt2

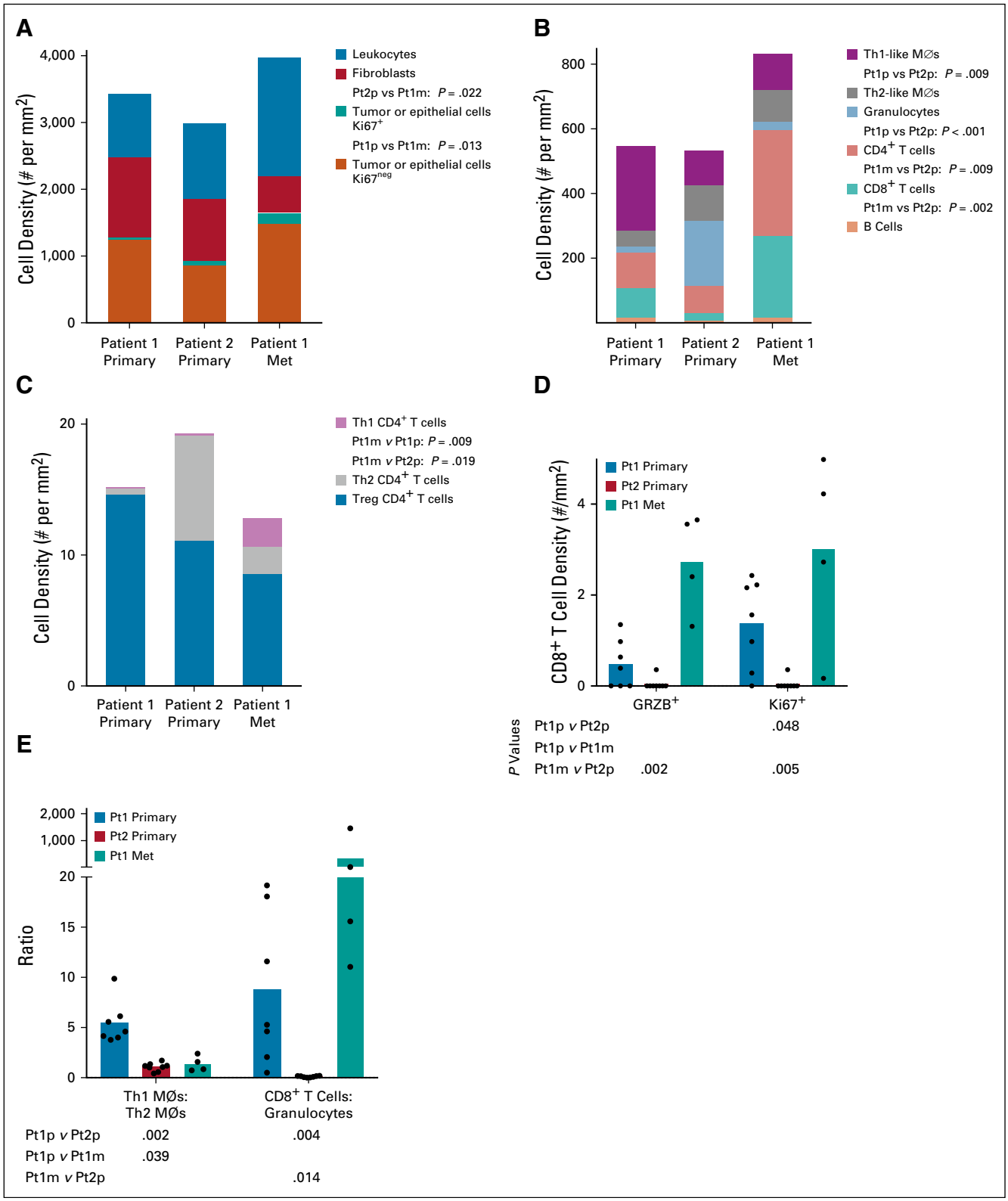

FIG 3. (A) Mean cell density per ROI for mutually exclusive populations of Ki67+ tumor or epithelial cells, Ki67neg tumor or epithelial cells, fibroblasts, and leukocytes. (B) Mean cell density per ROI of selected leukocyte types. (C) Mean cell density per ROI of mutually exclusive CD4+ T cell subsets. (D) Densities of CD8+GRZB+ and CD8+Ki67+ T cells. (E) Relative densities of Th1-like macrophages to Th2-like macrophages and CD8+ T cells to granulocytes. For D and E, each dot represents one ROI and column heights represent the mean of ROIs. All statistical comparisons between each of the three tumors for all cell types were tested by Kruskal-Wallis one-way ANOVA. Only *P* values < 0.05 are given. ANOVA, analysis of variance; ROI, region of interest.

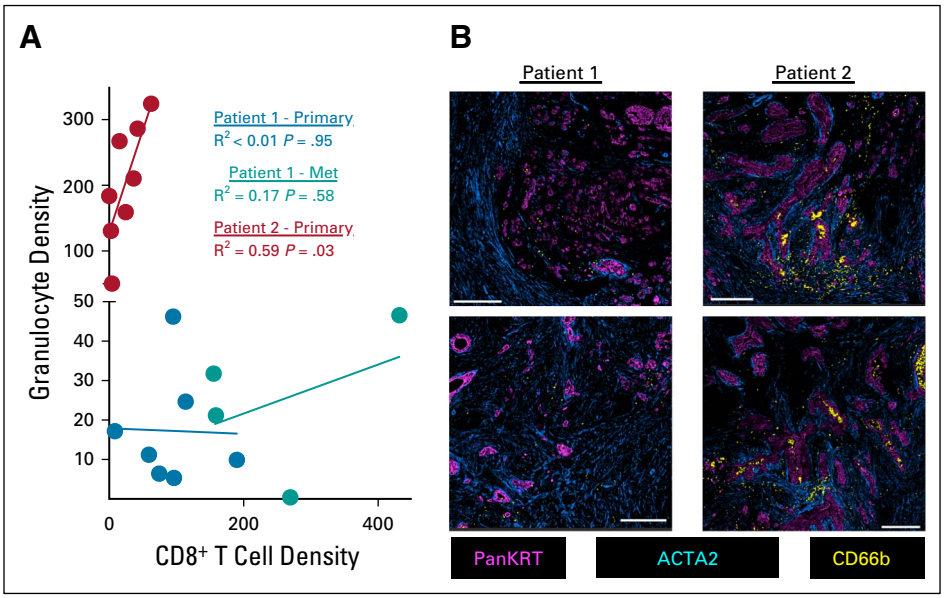

FIG 4. (A) Correlation between the densities of CD8⁺ T cells and granulocytes. Each dot represents one ROI. R^2 and *P* values are based on a simple linear regression. (B) Granulocytes (CD66b⁺), tumor cells (PanKRT⁺), and fibroblasts (ACTA2⁺) in primary tumors from each patient. Scale bars represent 250 μm. ROI, region of interest.

(Fig 3B). Among subsets of CD4⁺ T cells, we found more pro-inflammatory Th1 T cells in the metastasis from Pt1 than either primary tumor (Fig 3C). Neither Th2 nor Treg cells were significantly different among the tumors. Within CD4⁺ T cells, we found a greater density of both cytolytic granzyme B⁺ (GRZB) cells and proliferative Ki67⁺ cells in the metastasis from Pt1 than the primary tumor from Pt2 and a higher density of proliferative Ki67⁺ cells in Pt1's primary tumor compared with Pt2's primary tumor (Fig 3D). Consistent with the abundant Th1-like macrophages in Pt1's primary tumor, we found that the ratio of Th1-like to Th2-like macrophages was significantly greater in Pt1's primary tumor relative to the other 2 tumors (Fig 3E). A high granulocyte/neutrophil to lymphocyte ratio is associated with poor outcomes.[35,36] Consistent with this, the primary tumor from Pt2 had a significantly higher granulocyte to CD8⁺ T cell ratio than either tumor from Pt1 (Fig 3E). In addition, across ROIs, there was no correlation between the densities of CD8⁺ T cells and granulocytes in the tumors from Pt1, but there was a significant positive correlation in Pt2's primary tumor ($P < .03$, Fig 4A). Furthermore, the abundant granulocytes in Pt2's tumor were proximal to tumor cells and appeared within lumens (Fig 4B) where they may contribute to pathogenesis by occluding ducts.[37]

We also observed tertiary lymph structures (TLSs) at the border of both primary tumors, but these were more prevalent in the primary tumor from Pt1 (Appendix Fig A1). TLSs from Pt1 also contained significantly more B cells, CD4⁺ T cells, and CD8⁺ T cells (Appendix Fig A2) as previously reported for patients with relatively positive outcomes.[24,38]

Tissue Acquisition and Patient Consent

Human tissues were obtained with informed consent in accordance with the Declaration of Helsinki and were acquired through the Oregon Pancreas Tissue Registry under Oregon Health & Science University IRB protocol #3609.

DISCUSSION

We investigated multiple modalities and tumor characteristics of PDAC between two related patients. We found several similarities between both patients' cancers, including genes commonly altered in aggressive PDAC (*KRAS*, *TP53*, and *SMAD4*[39,40]) and a shared *PRSS1* A16V germline mutation that may predispose to pancreatitis[41-44] but is variably penetrant,[45] raising the possibility that this specific alteration leads to subclinical pancreatitis that accelerates tumorigenesis, consistent with Pt2's early onset of disease.[41,46]

The disease course for Pt1 was exceptional in the context of occult, chemotherapy-resistant metastatic disease for nearly 4 years. We identified several differences between Pt1 and Pt2 that may alone—or in combination—account for the divergent outcomes. An *FANCA* mutation in the metastasis from Pt1 might have sensitized that tumor to adjuvant gemcitabine and Xeloda and later to SBRT; however, Pt1's lung metastasis progressed during adjuvant chemotherapy, and no adjuvant treatment was given after surgical resection of the lung metastasis, suggesting that the indolent disease might have also been controlled by other factors. Both tumors from Pt2 contained an alteration in *CDKN2A*, and the metastasis from Pt2 had a copy number loss of *PTEN*; alterations in these genes are associated with poor outcomes and drug resistance.[47-49]

Pt1's classical subtype tumors and metastases limited to the lungs are both favorable prognostic factors. Patients with classical subtype tumors survive longer (25-30 months) than patients with basal-type tumors (10-15 months)[17-19] and are less likely to have recurrent, metastatic disease.[14,15] Patients with metastases restricted

to the lungs survive on average 23 months from diagnosis[8]; Pt1 has survived > 46 months with asymptomatic metastatic disease.

Our data link the indolent disease in Pt1 with reported indicators of tumor immunity. Specifically, more prevalent TLSs at the periphery of the primary tumor (Appendix Fig A1) and denser CD8+ T cells (Fig 3B) that did not correlate with the density of granulocytes[24,50] (Fig 4A), opening the possibility that tumor cells and/or CD4+ T cells in Pt1's tumors recruit fundamentally different leukocyte cell types from Pt2's tumors.[51] Additionally, granulocytes typically promote immunosuppression in late-stage tumors,[52] consistent with the relatively low number of T cells in Pt2's tumor.

Classical subtype PDAC with lung metastases and unconventional tumor immunity may lead to exceptional outcomes. Genetic analyses and tumor leukocyte phenotyping of larger cohorts of patients with PDAC lung metastases may reveal whether metastatic organotropism is modulated by tumor immunity and/or PDAC subtype.

METHODS

See Appendix 1, Supplemental Material.

AFFILIATIONS

[1]Department of Molecular and Medical Genetics, Oregon Health and Science University, Portland, OR
[2]Brenden-Colson Center for Pancreatic Care, Oregon Health and Science University, Portland, OR
[3]Department of Cell, Developmental, and Cancer Biology, Oregon Health & Science University, Portland, OR
[4]Computational Biology, Oregon Health and Science University, Portland, OR
[5]Department of Biomedical Engineering and OHSU Center for Spatial Systems Biomedicine, Oregon Health and Science University, Portland, OR
[6]Department of Pathology, Oregon Health and Science University, Portland, OR
[7]Department of Hematology and Oncology, Portland, OR
[8]Knight Cancer Institute, Portland, OR

CORRESPONDING AUTHOR

Rosalie C. Sears, PhD, Brenden-Colson Center for Pancreatic Care, Oregon Health and Science University, 2730 S Moody Ave, Portland, OR 97201; e-mail: searsr@ohsu.edu.

SUPPORT

Supported by the Brenden-Colson Foundation and NCI grant U01 CA224012 to R.C. Sears and L.M. Coussens; and a Brenden-Colson Center for Pancreatic Care pilot project grant to J.M. Link.

AUTHORS' DISCLOSURES OF POTENTIAL CONFLICTS OF INTEREST

The following represents disclosure information provided by authors of this manuscript. All relationships are considered compensated unless otherwise noted. Relationships are self-held unless noted. I = Immediate Family Member, Inst = My Institution. Relationships may not relate to the subject matter of this manuscript. For more information about ASCO's conflict of interest policy, please refer to www.asco.org/rwc or ascopubs.org/cci/author-center.

Open Payments is a public database containing information reported by companies about payments made to US-licensed physicians (Open Payments).

Carl R. Pelz
Consulting or Advisory Role, Immediate Family Member: Novartis

Charles D. Lopez
Consulting or Advisory Role: Boston Scientific, Celgene, Boston Biomedical, Pfizer, Exelixis, Astellas Pharma
Research Funding: Taiho Pharmaceutical
Travel, Accommodations, Expenses: RenovoRx

Lisa M. Coussens
Employment: Oregon Health & Science University (OHSU)
Honoraria: Prospect Creek Foundation, Lustgarten Foundation for Pancreatic Cancer Research, Syndax Pharmaceuticals, Inc: External Advisory Board, Carisma Therapeutics Inc: Scientific Advisory Board, Verseau Therapeutics, Inc, Scientific Advisory Board, Zymeworks, Inc, Scientific Advisory Board, CytomX Therapeutics, Inc, Kineta Inc, (P30) Koch Institute for Integrated Cancer Research, Massachusetts Inst. of Tech, (P30) Salk Institute Cancer Center, Bloomberg-Kimmel Institute for Cancer Immunotherapy, Sidney Kimmel Comprehensive Cancer Center at Johns Hopkins, Dana Farber Cancer Center Breast SPORE, (P30) Dana Farber/Harvard Cancer Center, (P30) University of California, San Diego Moores Cancer Center, Starr Cancer Consortium, Lustgarten Foundation for Pancreatic Cancer Research, Therapeutics Working Group, NIH/NCI-Frederick National Laboratory Advisory Committee (FNLAC), Susan G Komen Foundation, Komen Scholar
Consulting or Advisory Role: Cell Signaling Technologies, Pharmacyclics, CytomX Therapeutics, Syndax, Carisma Therapeutics, Verseau Therapeutics, Zymeworks, Kineta, Inc, Abbvie, Shasqi Inc
Research Funding: Syndax Pharmaceuticals Inc, Pharmacyclics, Cell Signaling Technologies, Innate Pharma, Deciphera
Travel, Accommodations, Expenses: Cell Signaling Technologies, AstraZeneca, Pharmacyclics, Verseau, Carisma Therapeutics, CytomX Therapeutics, Zymeworks
Other Relationship: Prospect Creek Foundation, Lustgarten Foundation for Pancreatic Cancer Research, (P30) Koch Institute for Integrated Cancer Research, Massachusetts Inst. of Tech. (2012-present; honorarium), (P30) Salk Institute Cancer Center: (2016-2020; honorarium), Bloomberg-Kimmel Institute for Cancer Immunotherapy, Sidney Kimmel Comprehensive Cancer Center at Johns Hopkins: (2016-present; honorarium), Dana Farber Cancer Center Breast SPORE: (2017-present; honorarium), (P30) Dana Farber/Harvard Cancer Center: (2019-present; honorarium), (P30) University of California, San Diego Moores Cancer Center (2019-present; honorarium), Cancer Research Institute (CRI): (2013-present; unpaid), The V Foundation for Cancer Research): (2013-present; unpaid), Starr Cancer Consortium: (2011-present, honorarium), Lustgarten Foundation for Pancreatic Cancer Research, Therapeutics Working Group: (2019-present; paid), NIH/NCI-Frederick National Laboratory Advisory Committee (FNLAC): (2016-present; daily honorarium), Susan G Komen Foundation, Komen Scholar (2020 – 2023; honorarium)

Rosalie C. Sears
Consulting or Advisory Role: Novartis

No other potential conflicts of interest were reported

AUTHOR CONTRIBUTIONS

Conception and design: Jason M. Link, Courtney B. Betts, Charles D. Lopez, Lisa M. Coussens, Rosalie C. Sears

Financial support: Lisa M. Coussens, Rosalie C. Sears
Administrative support: Dove Keith
Provision of study materials or patients: Lisa M. Coussens
Collection and assembly of data: Jason M. Link, Shannon M. Liudahl, Kenna R. Leis, Mary McDonnell, Brett Johnson, Kelly J. Hamman, Dove Keith, Terry K. Morgan, Charles D. Lopez, Lisa M. Coussens, Rosalie C. Sears
Data analysis and interpretation: Jason M. Link, Shannon M. Liudahl, Courtney B. Betts, Shamilene Sivagnanam, Carl R. Pelz, Brett Johnson, Kelly J. Hamman, Jone E. Sampson, Charles D. Lopez, Lisa M. Coussens, Rosalie C. Sears
Manuscript writing: All authors
Final approval of manuscript: All authors
Accountable for all aspects of the work: All authors

REFERENCES

1. Hidalgo M, Cascinu S, Kleeff J, et al: Addressing the challenges of pancreatic cancer: Future directions for improving outcomes. Pancreatology 15:8-18, 2015
2. Cancer Facts & Figures 2018. American Cancer Society, 2018. https://www.cancer.org/research/cancer-facts-statistics/all-cancer-facts-figures/cancer-facts-figures-2018.html
3. Conroy T, Hammel P, Hebbar M, et al: FOLFIRINOX or gemcitabine as adjuvant therapy for pancreatic cancer. N Engl J Med 379:2395-2406, 2018
4. Iacobuzio-Donahue CA, Fu B, Yachida S, et al: DPC4 gene status of the primary carcinoma correlates with patterns of failure in patients with pancreatic cancer. J Clin Oncol 27:1806-1813, 2009
5. Yachida S, Jones S, Bozic I, et al: Distant metastasis occurs late during the genetic evolution of pancreatic cancer. Nature 467:1114-1117, 2010
6. Makohon-Moore AP, Zhang M, Reiter JG, et al: Limited heterogeneity of known driver gene mutations among the metastases of individual patients with pancreatic cancer. Nat Genet 49:358-366, 2017
7. Katz MHG, Wang H, Fleming JB, et al: Long-term survival after multidisciplinary management of resected pancreatic adenocarcinoma. Ann Surg Oncol 16:836-847, 2009
8. Downs-Canner S, Zenati M, Boone BA, et al: The indolent nature of pulmonary metastases from ductal adenocarcinoma of the pancreas. J Surg Oncol 112:80-85, 2015
9. Deeb A, Haque SU, Olowokure O: Pulmonary metastases in pancreatic cancer, is there a survival influence? J Gastrointest Oncol 6:E48-E51, 2015
10. Yasukawa M, Kawaguchi T, Kawai N, et al: Surgical treatment for pulmonary metastasis of pancreatic ductal adenocarcinoma: Study of 12 cases. Anticancer Res 37:5573-5576, 2017
11. Follia L, Ferrero G, Mandili G, et al: Integrative analysis of novel metabolic subtypes in pancreatic cancer fosters new prognostic biomarkers. Front Oncol 9:115, 2019
12. Daemen A, Peterson D, Sahu N, et al: Metabolite profiling stratifies pancreatic ductal adenocarcinomas into subtypes with distinct sensitivities to metabolic inhibitors. Proc Natl Acad Sci U S A 112:E4410-E4417, 2015
13. Chan-Seng-Yue M, Kim JC, Wilson GW, et al: Transcription phenotypes of pancreatic cancer are driven by genomic events during tumor evolution. Nat Genet 52:231-240, 2020
14. Connor AA, Denroche RE, Jang GH, et al: Integration of genomic and transcriptional features in pancreatic cancer reveals increased cell cycle progression in metastases. Cancer Cell 35:267-282.e7, 2019
15. Puleo F, Nicolle R, Blum Y, et al: Stratification of pancreatic ductal adenocarcinomas based on tumor and microenvironment features. Gastroenterology 155:1999-2013.e3, 2018
16. Somerville TD, Biffi G, Daßler-Plenker J, et al: Squamous trans-differentiation of pancreatic cancer cells promotes stromal inflammation. eLife 9:e53381, 2020
17. Bailey P, Chang DK, Nones K, et al: Genomic analyses identify molecular subtypes of pancreatic cancer. Nature 531:47-52, 2016
18. Collisson EA, Sadanandam A, Olson P, et al: Subtypes of pancreatic ductal adenocarcinoma and their differing responses to therapy. Nat Med 17:500-503, 2011
19. Raphael BJ, Hruban RH, Aguirre AJ, et al: Integrated genomic characterization of pancreatic ductal adenocarcinoma. Cancer Cell 32:185-203.e13, 2017
20. de Santiago I, Yau C, Heij L, et al: Immunophenotypes of pancreatic ductal adenocarcinoma: Meta-analysis of transcriptional subtypes. Int J Cancer 145:1125-1137, 2019
21. Moffitt RA, Marayati R, Flate EL, et al: Virtual microdissection identifies distinct tumor- and stroma-specific subtypes of pancreatic ductal adenocarcinoma. Nat Genet 47:1168-1178, 2015
22. Knudsen ES, Vail P, Balaji U, et al: Stratification of pancreatic ductal adenocarcinoma: Combinatorial genetic, stromal, and immunologic markers. Clin Cancer Res 23:4429-4440, 2017
23. Balli D, Rech AJ, Stanger BZ, et al: Immune cytolytic activity stratifies molecular subsets of human pancreatic cancer. Clin Cancer Res 23:3129-3138, 2017
24. Stromnes IM, Hulbert A, Pierce RH, et al: T-cell localization, activation, and clonal expansion in human pancreatic ductal adenocarcinoma. Cancer Immunol Res 5:978-991, 2017
25. Balachandran VP, Łuksza M, Zhao JN, et al: Identification of unique neoantigen qualities in long-term survivors of pancreatic cancer. Nature 551:512-516, 2017
26. Gunderson AJ, Kaneda MM, Tsujikawa T, et al: Bruton's tyrosine kinase (BTK)-dependent immune cell crosstalk drives pancreas cancer. Cancer Discov 6:270-285, 2016
27. Joyce JA, Fearon DT: T cell exclusion, immune privilege, and the tumor microenvironment. Science 348:74-80, 2015
28. Bauer C, Kühnemuth B, Duewell P, et al: Prevailing over T cell exhaustion: New developments in the immunotherapy of pancreatic cancer. Cancer Lett 381:259-268, 2016
29. Gunderson AJ, Coussens LM: B cells and their mediators as targets for therapy in solid tumors. Exp Cell Res 319:1644-1649, 2013
30. Stromnes IM, Brockenbrough JS, Izeradjene K, et al: Targeted depletion of a MDSC subset unmasks pancreatic ductal adenocarcinoma to adaptive immunity. Gut 63:1769-1781, 2014
31. Li J, Byrne KT, Yan F, et al: Tumor cell-intrinsic factors underlie heterogeneity of immune cell infiltration and response to immunotherapy. Immunity 49:178-193.e7, 2018
32. Hayashi A, Fan J, Chen R, et al: A unifying paradigm for transcriptional heterogeneity and squamous features in pancreatic ductal adenocarcinoma. Nat Cancer 1:59-74, 2020

33. Rashid NU, Peng XL, Jin C, et al: Purity independent subtyping of tumors (PurIST), A clinically robust, single-sample classifier for tumor subtyping in pancreatic cancer. Clin Cancer Res 26:82-92, 2020
34. Tsujikawa T, Kumar S, Borkar RN, et al: Quantitative multiplex immunohistochemistry reveals myeloid-inflamed tumor-immune complexity associated with poor prognosis. Cell Rep 19:203-217, 2017
35. Zhou Y, Wei Q, Fan J, et al: Prognostic role of the neutrophil-to-lymphocyte ratio in pancreatic cancer: A meta-analysis containing 8252 patients. Clin Chim Acta 479:181-189, 2018
36. Giakoustidis A, Neofytou K, Costa Neves M, et al: Identifying the role of neutrophil-to-lymphocyte ratio and platelets-to-lymphocyte ratio as prognostic markers in patients undergoing resection of pancreatic ductal adenocarcinoma. Ann Hepatobiliary Pancreat Surg 22:197-207, 2018
37. Leppkes M, Maueröder C, Hirth S, et al: Externalized decondensed neutrophil chromatin occludes pancreatic ducts and drives pancreatitis. Nat Commun 7:10973-11013, 2016
38. Lutz ER, Wu AA, Bigelow E, et al: Immunotherapy converts nonimmunogenic pancreatic tumors into immunogenic foci of immune regulation. Cancer Immunol Res 2:616-631, 2014
39. Blackford A, Serrano OK, Wolfgang CL, et al: SMAD4 gene mutations are associated with poor prognosis in pancreatic cancer. Clin Cancer Res 15:4674-4679, 2009
40. Herman JM, Jabbour SK, Lin SH, et al: Smad4 loss correlates with higher rates of local and distant failure in pancreatic adenocarcinoma patients receiving adjuvant chemoradiation. Pancreas 47:208-212, 2018
41. Rebours V, Boutron-Ruault MC, Schnee M, et al: Risk of pancreatic adenocarcinoma in patients with hereditary pancreatitis: A national exhaustive series. Am J Gastroenterol 103:111-119, 2008
42. Weiss FU: Pancreatic cancer risk in hereditary pancreatitis. Front Physiol 5:70, 2014
43. Schubert S, Traub F, Brakensiek K, et al: CFTR, SPINK1, PRSS1, and CTRC mutations are not associated with pancreatic cancer in German patients. Pancreas 43:1078, 2014
44. Teich N, Rosendahl J, Tóth M, et al: Mutations of human cationic trypsinogen (PRSS1) and chronic pancreatitis. Hum Mutat 27:721-730, 2006
45. Grocock CJ, Rebours V, Delhaye MN, et al: The variable phenotype of the p.A16V mutation of cationic trypsinogen (PRSS1) in pancreatitis families. Gut 59:357-363, 2010
46. McWilliams RR, Maisonneuve P, Bamlet WR, et al: Risk factors for early-onset and very-early-onset pancreatic adenocarcinoma: A pancreatic cancer case-control consortium (PanC4) analysis. Pancreas 45:311-316, 2016
47. Kim M, Shah A, Zhang J, et al: Gemcitabine resistance in cultured pancreatic tumor cells is associated with down regulation of PTEN and a mesenchymal phenotype. Cancer Res 68:2460, 2008
48. Ferrer M, de Winter JP, Mastenbroek DC, et al: Chemosensitizing tumor cells by targeting the Fanconi anemia pathway with an adenovirus overexpressing dominant-negative FANCA. Cancer Gene Ther 11:539-546, 2004
49. Doyle A, Kubler MM, Harris AC, et al: The impact of CDKN2A mutations on overall survival in pancreatic adenocarcinoma. J Clin Oncol 37:278, 2019
50. Chao T, Furth EE, Vonderheide RH: CXCR2-Dependent accumulation of tumor-associated neutrophils regulates T-cell immunity in pancreatic ductal adenocarcinoma. Cancer Immunol Res 4:968-982, 2016
51. SenGupta S, Subramanian BC, Parent CA: Getting TANned: How the tumor microenvironment drives neutrophil recruitment. J Leukoc Biol 105:449-462, 2019
52. Lecot P, Sarabi M, Pereira Abrantes M, et al: Neutrophil heterogeneity in cancer: From biology to therapies. Front Immnuol 10:2155, 2019
53. Corless CL: Next-generation sequencing in cancer diagnostics. J Mol Diagn 18:813-816, 2016
54. Mitri ZI, Parmar S, Johnson B, et al: Implementing a comprehensive translational oncology platform: From molecular testing to actionability. J Transl Med 16:358, 2018
55. Li H, Durbin R: Fast and accurate short read alignment with Burrows–Wheeler transform. Bioinformatics 25:1754-1760, 2009
56. McKenna A, Hanna M, Banks E, et al: The Genome Analysis Toolkit: A MapReduce framework for analyzing next-generation DNA sequencing data. Genome Res 20:1297-1303, 2010
57. DePristo MA, Banks E, Poplin R, et al: A framework for variation discovery and genotyping using next-generation DNA sequencing data. Nat Genet 43:491-498, 2011
58. Cibulskis K, Lawrence M, Carter SL, et al: Sensitive detection of somatic point mutations in impure and heterogeneous cancer samples. Nat Biotechnol 31:213-219, 2013
59. Ye K, Schulz MH, Long Q, et al: Pindel: A pattern growth approach to detect break points of large deletions and medium sized insertions from paired-end short reads. Bioinformatics 25:2865-2871, 2009
60. Robinson JT, Thorvaldsdottir H, Winckler W, et al: Integrative genomics viewer. Nat Biotechnol 29:24-26, 2011
61. Talevich E, Shain AH, Botton T, et al: CNVkit: Genome-wide copy number detection and visualization from targeted DNA sequencing. PLoS Comput Biol 12:e1004873, 2016
62. Daemen A, Griffith OL, Heiser LM, et al: Modeling precision treatment of breast cancer. Genome Biol 14:R110, 2013
63. Langmead B, Trapnell C, Pop M, et al: Ultrafast and memory-efficient alignment of short DNA sequences to the human genome. Genome Biol 10:R25, 2009
64. Carpenter AE, Jones TR, Lamprecht MR, et al: CellProfiler: Image analysis software for identifying and quantifying cell phenotypes. Genome Biol 7:R100, 2006
65. Chan A, Prassas I, Dimitromanolakis A, et al: Validation of biomarkers that complement CA19.9 in detecting early pancreatic cancer. Clin Cancer Res 20:5787-5795, 2014

APPENDIX 1. SUPPLEMENTAL METHODS

Tumor Somatic Alterations

Somatic alterations were identified by the Knight Diagnostics Lab at Oregon Health & Science University as previously described[53,54] using the GeneTrails® Comprehensive Solid Tumor Panel.

Germline variants identified by whole exome sequencing

Genomic DNA was isolated from 10 μm tumor sections macrodissected to enrich for tumor cells. Exome sequencing libraries were prepared with a KAPA Hyper Prep Kit, enriched using the Agilent SureSelectXT Clinical Research Exome, and paired-end sequenced with an Illumina HiSeq 2500 to a high depth of 300 ×. Tumor and autologous normal blood cell whole exome sequencing (WES) data were compared to identify tumor-specific somatic alterations. WES data were processed by aligning reads to the human genome using the Burrows-Wheeler Aligner (bwa)[55] and removing duplicate reads with Picard (http://broadinstitute.github.io/picard). Base quality recalibration and small insertion and deletion (indel) realignment were performed using the Genome Analysis Toolkit (GATK).[56,57] Single-nucleotide variants (SNVs) were identified by MuTect[58], and indels were identified using Pindel.[59] All somatic mutation cells were manually reviewed using the Integrative Genomics Viewer.[60] Somatic copy number alterations were identified by comparing exome sequencing coverage levels in each sample with those in a pool of normal exomes using the CNVkit algorithm.[61]

RNA Sequencing and Analysis

RNA was isolated from 10 μm tumor sections macrodissected to enrich for at least 40% tumor cells. RNA sequencing was performed as previously reported.[62] Briefly, RNA was extracted using an RNeasy Kit (Qiagen) and evaluated by the OHSU Massively Parallel Sequencing Shared Resource (MPSSR) core facility for library construction with the TruSeq RNA Access Library Prep Kit (Illumina). All RNA samples had a %DV200 > 30% as measured using an Agilent 2100 Bioanalyzer. RNA was sequenced on an Illumina HiSeq 2500/4000 to generate 100 bp paired-end reads for a minimum depth of 40 million reads per sample. RNAseq data were preprocessed using Illumina Sequencing Control Software and CASAVA v1.8 to produce demultiplexed fastq files (http://broadinstitute.github.io/picard). The Bowtie alignment algorithm was used for read realignment to the hg19 human genome.[63] UCSC Refseq gene annotations were used to calculate FPKM values.

For gene expression–based subtype assignment, we use the PDAssigner gene list and the average rank order of expression for these genes in published human PDAC samples previously designated as classical or quasimesenchymal.[18] Gene expression of tumor samples from Pt1 and Pt2 was normalized to each other by calculating z-scores. We determined the Spearman rank-order correlation coefficient by comparing the average rank of the PDAssigner genes in the previously published classical and quasimesenchymal tumors with the rank of these genes in each of the four tumor samples from Pt1 and Pt2. We followed the published protocol for PurIST subtyping[33] and used the same data set as for PDAssigner subtyping.

Tissue processing and immunostaining

Tumor tissue samples were fixed in 10% neutral buffered formalin for 24 hours and embedded in paraffin (FFPE). Five micrometer FFPE tissue sections were affixed to glass slides and incubated at 55°C for 12 hours and then deparaffinized with xylene. Antigen retrieval was performed with both pH 6.0 and pH 9.0 buffers under high heat and pressure. FFPE sections were stained with hematoxylin and eosin, and KRT5 was detected with a rabbit monoclonal antibody (EP1601Y, Abcam) and polyclonal goat anti-rabbit antibodies (Invitrogen). Images were acquired with a Zeiss Axio Scan Slide Scanner. Exposure times and signal thresholds were normalized across all images.

Multiplex Immunohistochemistry, Image Acquisition, and Processing

Multiplex IHC was performed on 5 μm FFPE sections using an adapted protocol based on methodology we previously described.[34] Briefly, slides were deparaffinized and stained with hematoxylin (S3301, Dako, Santa Clara, CA), followed by whole slide scanning at 20 × magnification on an Aperio AT2 (Leica Biosystems, Wetzlar, Germany). Tissues were then subjected to 15 minutes of heat-mediated antigen retrieval in pH 6.0 Citra solution (BioGenex, Fremont, CA), 10 minutes of blocking in Dako Dual Endogenous Enzyme Block (S2003, Dako, Santa Clara, CA), and then 10 minutes of protein blocking with 5% normal goat serum and 2.5% BSA in TBST. Primary antibody details, dilution, and incubation times are listed in Appendix Tables A1 and A2. After washing off primary antibody in TBST, anti-rat, anti-mouse, or anti-rabbit Histofine Simple Stain MAX PO horseradish peroxidase (HRP)–conjugated polymer (Nichirei Biosciences, Tokyo, Japan) was applied for 30 minutes at room temperature, followed by AEC chromogen (Vector Laboratories, Burlingame, CA). Slides were digitally scanned following each chromogen development.

Scanned images were registered in MATLAB version R2018b using the SURF algorithm in the Computer Vision Toolbox (The MathWorks, Inc, Natick, MA). Image processing and cell quantification were performed using FIJI (FIJI Is Just ImageJ) CellProfiler Version 3.5.1[64] and FCS Express 6 Image Cytometry RUO (De Novo Software, Glendale, CA). AEC signal was extracted for quantification and visualization in FIJI using a custom macro for color deconvolution. Briefly, the FIJI plugin Color_Deconvolution [H AEC] was used to separate hematoxylin, followed by postprocessing steps for signal cleaning and background elimination. AEC signal was extracted in FIJI using the NIH plugin RGB_to_CMYK. Color deconvoluted images were processed in CellProfiler to quantify single-cell mean intensity signal measurements for every stained marker. Cells were classified based on hierarchical gating (image cytometry) and defined as described in Appendix Table A2. For visualization of CD45 and PanKRT staining, signal-extracted images were overlaid in pseudocolor in FIJI. QiTissue (Quantitative Imaging Systems) was used to generate pseudocolored images for Figure 4.

Statistics

Leukocyte types were analyzed if each tumor sample had an average of > 10 events per region of interest and if the average cell density for any tumor was > 1% of all leukocytes. Kruskal-Wallis one-way analysis of variance tests were performed using GraphPad Prism.

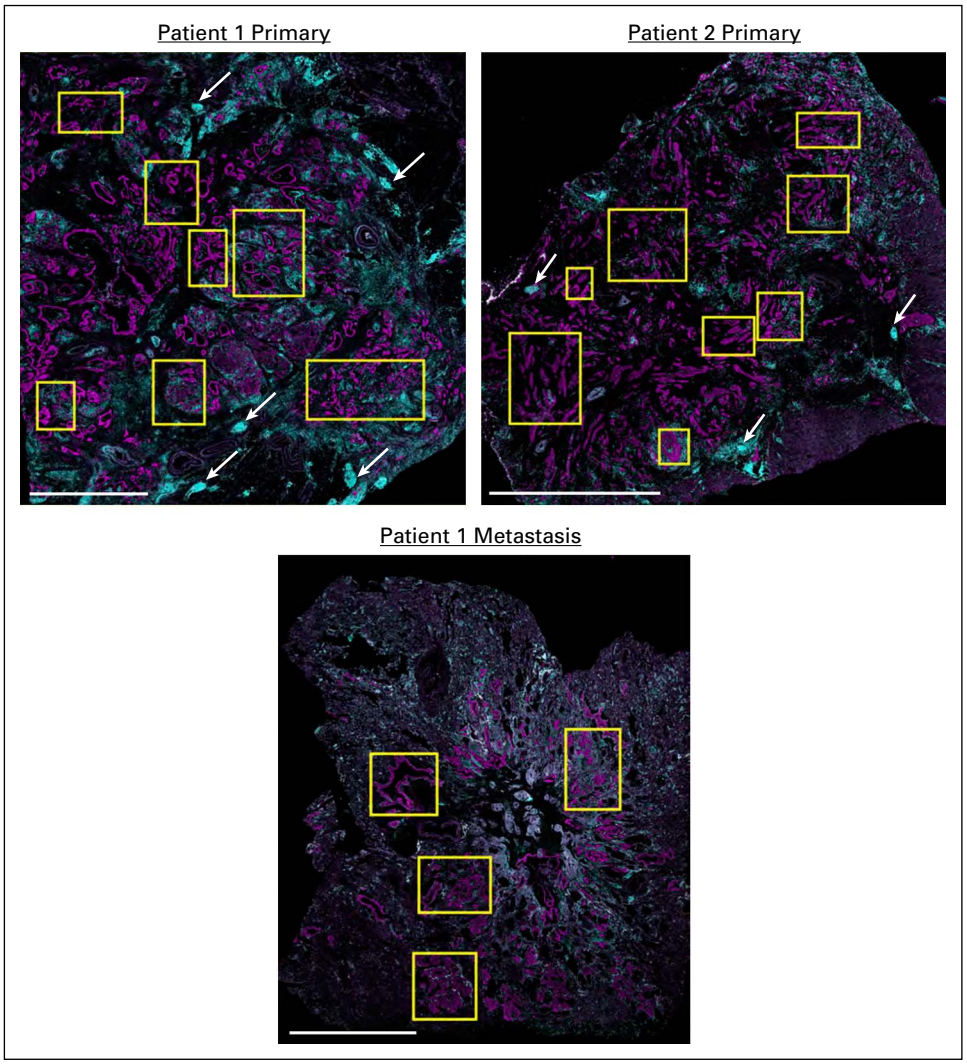

FIG A1. (A) KRT (magenta) and CD45 (teal) expression and selected ROIs (yellow rectangles) used for mIHC analyses of tumors (scale bars represent 5 mm). Examples of tertiary lymph structures (TLSs) are indicated with white arrows. ROIs, regions of interest.

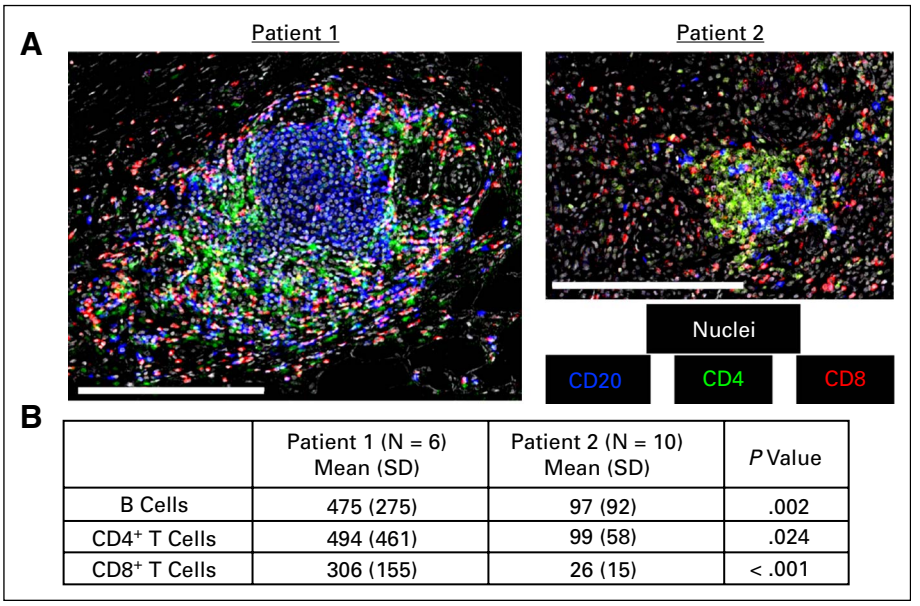

	Patient 1 (N = 6) Mean (SD)	Patient 2 (N = 10) Mean (SD)	*P* Value
B Cells	475 (275)	97 (92)	.002
$CD4^+$ T Cells	494 (461)	99 (58)	.024
$CD8^+$ T Cells	306 (155)	26 (15)	< .001

FIG A2. (A) Representative images of lymphocytes within TLSs. Scale bars represent 250 μm. (B) Mean number of B cells, $CD4^+$ T cells, and $CD8^+$ T cells within ROIs containing TLSs. *P* values are derived from a 2-tailed *t* test. ROIs, regions of interest; TLS, tertiary lymph structure.

TABLE A1. Antibodies and Targets Used in mIHC to Identify Phenotypes and Functions of Leukocytes

Target	PanKRT	ACTA2	CD45	CD3	CD8	Ki67	GZMB	T-bet	GATA-3	FOXP3	CD20	CD66b	Tryptase	CD68	CD163
Vendor	Abcam	Abcam	Thermo Fisher	Thermo Fisher	Thermo Fisher	Cell Marque	Abcam	Cell Signaling	BioCare	eBioscience	Abcam	BD Pharmingen	Abcam	Abcam	Thermo Fisher
Clone	AE1/AE3	Polyclonal	H130	SP7	C8/144B	SP6	Polyclonal	D6N8B	L50-823	236A/E7	SP32	G10F5	AA1	PG-M1	10D6
Dilution	1:2,000	1:200	1:100	1:150	1:100	1:500	1:200	1:500	1:50	1:40	1:1,000	1:200	1:20,000	1:50	1:100
Incubation	30 min at RT	30 min at RT	1 hr at RT	1 hr at RT	30 min at RT	30 min at RT	ON at 4C	ON at 4C	ON at 4C	30 min at RT	1 hr at RT	30 min at RT	30 min at RT	30 min at RT	30 min at RT

TABLE A2. Target Combinations Used to Define the Leukocyte Types Reported

Cell Types Identified by mIHC	
Epithelial or tumor cells	KRT^{+} $ACTA2^{neg}$ $CD45^{neg}$
Fibroblasts	KRT^{neg} $ACTA2^{+}$ $CD45^{neg}$
Leukocytes	KRT^{neg} $ACTA2^{neg}$ $CD45^{+}$
Leukocyte Subsets	**All Cell Types Below are KRT^{neg} $ACTA2^{neg}$ $CD45^{+}$**
$CD8^{+}$ T lymphocytes	$CD3^{+}$ $CD8^{+}$ $CD68^{neg}$
$CD4^{+}$ T lymphocytes	$CD3^{+}$ $CD8^{neg}$ $CD68^{neg}$
Th1 helper T cells	$CD3^{+}$ $CD8^{neg}$ T-bet^{+} GATA-3^{neg} $FOXP3^{neg}$ $CD68^{neg}$
Th2 helper T cells	$CD3^{+}$ $CD8^{neg}$ T-bet^{neg} GATA-3^{+} $FOXP3^{neg}$ $CD68^{neg}$
Regulatory T cells (Treg)	$CD3^{+}$ $CD8^{neg}$ T-bet^{neg} GATA-3^{neg} $FOXP3^{+}$ $CD68^{neg}$
B cells	$CD20^{+}$ $CD3^{neg}$ $CD68^{neg}$
Granulocytes	$CD3/CD20^{neg}$ $Tryptase^{neg}$ $CD66b^{+}$
Macrophages	$CD3/CD20^{neg}$ $CD66b^{neg}$ $Tryptase^{neg}$ $CD68^{+}$
Th1-like macrophages	$CD3/CD20^{neg}$ $CD66b^{neg}$ $Tryptase^{neg}$ $CD68^{+}$ $CD163^{neg}$
Th2-like macrophages	$CD3/CD20^{neg}$ $CD66b^{neg}$ $Tryptase^{neg}$ $CD68^{+}$ $CD163^{+}$

